Accepted Manuscript

Elucidation of Cold-Spray Deposition Mechanism by Auger Electron Spectroscopic Evaluation of Bonding Interface Oxide Film

Yuji Ichikawa, Ryotaro Tokoro, Masatoshi Tanno, Kazuhiro Ogawa

PII: S1359-6454(18)30753-5

DOI: 10.1016/j.actamat.2018.09.041

Reference: AM 14850

To appear in: *Acta Materialia*

Received Date: 27 March 2018

Revised Date: 18 September 2018

Accepted Date: 18 September 2018

Please cite this article as: Y. Ichikawa, R. Tokoro, M. Tanno, K. Ogawa, Elucidation of Cold-Spray Deposition Mechanism by Auger Electron Spectroscopic Evaluation of Bonding Interface Oxide Film, *Acta Materialia* (2018), doi: https://doi.org/10.1016/j.actamat.2018.09.041.

This is a PDF file of an unedited manuscript that has been accepted for publication. As a service to our customers we are providing this early version of the manuscript. The manuscript will undergo copyediting, typesetting, and review of the resulting proof before it is published in its final form. Please note that during the production process errors may be discovered which could affect the content, and all legal disclaimers that apply to the journal pertain.

Graphical Abstract

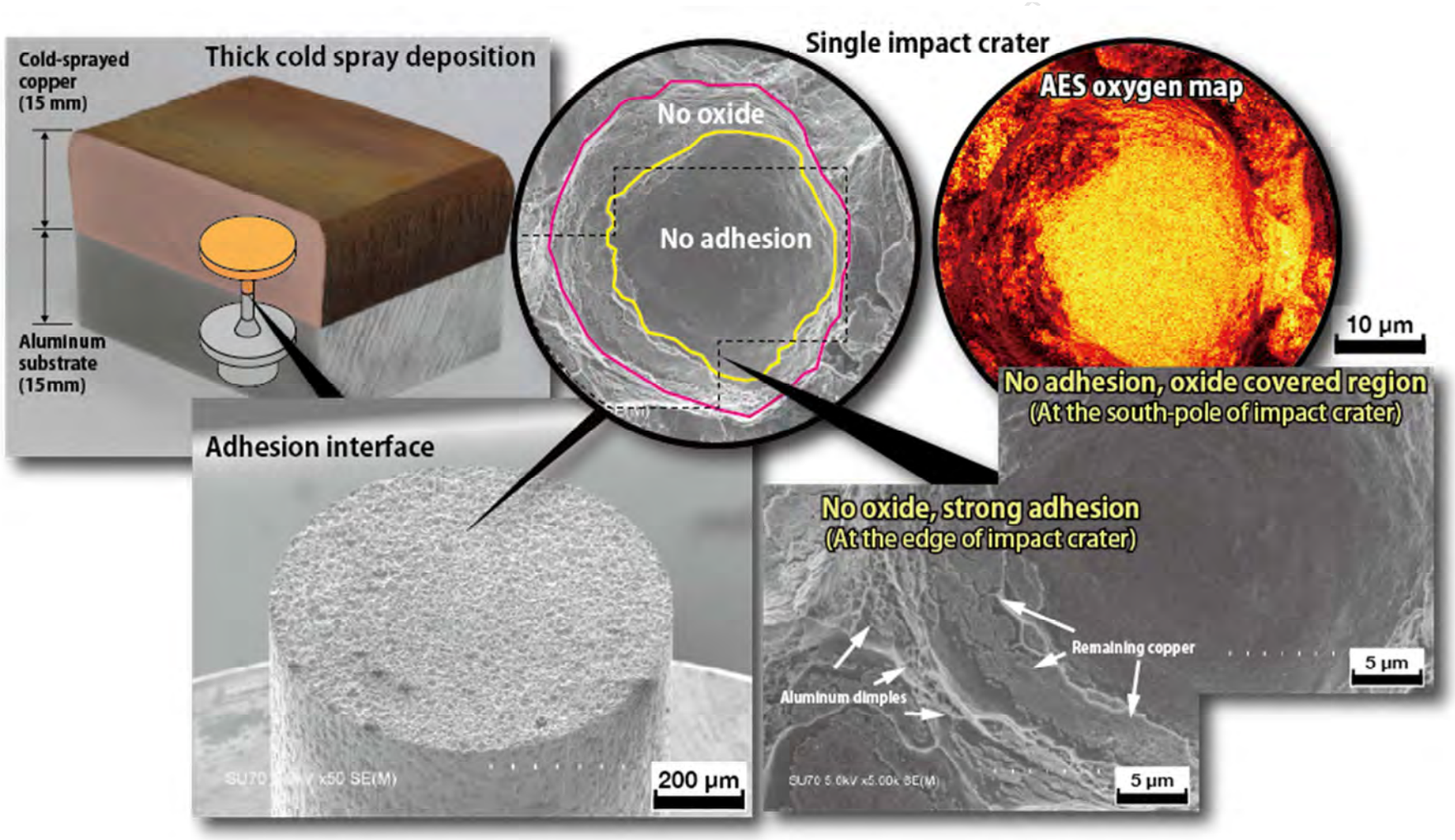

ACCEPTED MANUSCRIPT

Elucidation of Cold-Spray Deposition Mechanism by Auger Electron Spectroscopic Evaluation of Bonding Interface Oxide Film

Yuji Ichikawa*, Ryotaro Tokoro, Masatoshi Tanno, and Kazuhiro Ogawa

Tohoku University, 6-6-11-703, Aoba, Aramaki, Aoba-ku, Sendai 980-8579, Japan

*Corresponding author (Tel: +81-22-795-6933, E-mail: ichikawa@rift.mech.tohoku.ac.jp)

Keywords

Cold Spray, Auger Electron Spectroscopy, Adhesion Strength, Oxide, South-Pole Problem

Abstract

The relationship between the cold spray deposition mechanism, microstructure, and strength of the resulting film must be understood for this innovative process to be practical. Previous studies have suggested that the coating mechanism is reliant on breaking the natural oxide film such that metallic bonding occurs through direct contact between the metal surfaces. In this study, the proposed model was experimentally verified by a small tensile adhesion test and auger electron spectroscopy analysis of the bonding interface. Since shear deformation does not occur at the tip (south pole) of the incoming particle, the oxide film is not broken, such that the bonding strength is weak. In contrast, at the outer edge of the particle, metallic bonding occurs, attaining a level of strength that exceeds that of the base material due to the huge plastic deformation. This phenomenon is known as the “south-pole problem,” and can lead to a decrease in the overall adhesion strength despite the local adhesion being strong. However, detailed observations revealed, in parts of the deposits,

ACCEPTED MANUSCRIPT

particles that had adhered across their entire surface. This suggests that, provided the collision state can be controlled, it is possible to overcome the south-pole problem and improve the adhesion strength.

1. Introduction

The cold-spray (CS) method is a completely new particle deposition method [1–3]. The most important feature of this method is that the particles are not melted. That is, metallic particles with a diameter of several micro-meters to several tens of micro-meters impact a substrate and, while remaining solid, form a deposit that can be built up into a layer with a thickness of several tens of micro-meters to several centimeters. The process does not involve the melting of the metal, and offers many advantages as a result of being fundamentally different from conventional thermal-spraying methods. Therefore, it is expected to be adopted as a next-generation surface-modification and additive manufacturing technology [4,5].

The most interesting aspect of the process is that particles in the solid phase collide with and combine, first with the substrate and then with each other, such that a relatively thick layer can be formed. Many studies have addressed this deposition mechanism [6–33]. Many of these efforts have addressed the elementary process whereby particles impact, deform, and adhere. Various kinds of the adhere models have also been proposed. The so-called “oxide break deposition model” has been proposed whereby contact occurs between the newly generated surfaces that are formed by the destruction and removal of the native oxide film upon impact, as shown in **Fig. 1**. The kinetic energy of the particles, accelerated to high speed, is converted into the large plastic deformation of the metallic particles and the substrate material at the instant of the collision. The natural oxide films covering the particle and the substrate surfaces are destroyed, and the exposed metallic surfaces come into contact with each other to form metallic bonds [34,35]. Previous experimental results proved that the oxide film on the substrate is an important factor influencing the deposition

ACCEPTED MANUSCRIPT

efficiency of the cold spray method. We regard this as being a convincing model [35–39]. Another phenomenon supporting this model is known as the "south-pole problem" [26,30,40,41]. As can be seen in Fig. 1, the particles and the substrate undergo shear deformation at the point of collision.

At the outer periphery of each particle, the shear plastic deformation that occurs is of such a large degree that it forms a plastic flow that is called a "material jet." On the other hand, the amount of shear plastic deformation falls to zero at the initial point of collision, when perpendicular to the substrate material, that is, the south pole part of the particle. For this reason, the oxide film at the south pole remains as is without being destroyed. If adhesion with the cold-spray method depends on the removal of the oxide film to form new surfaces, which then come into contact with each other to form a metallic bond, adhesion does not occur at the south pole of the particle. Although this is an analytically understandable phenomenon, it is difficult to discuss based only on the experimental results, because the oxide film is too thin to analyze using scanning electron microscopy with energy-dispersive X-ray spectroscopy (SEM-EDX) [42].

The adhesion strength is one of the most important properties affecting the reliability of the cold-spray coating and deposition [43–45]. It is impossible to consider this adhesion strength separately from the deposition mechanism. Considering the mechanism, including the above-mentioned south-pole problem, it is unlikely that the particles adhering to the substrate will exhibit a uniform level of strength, with the local strength varying greatly depending on the location. Understanding the overall adhesion strength of the deposition and establishing a strength prediction model is therefore very important if the cold-spray technique is to attract widespread adoption.

The interfacial adhesion strength between cold-sprayed copper and aluminum substrate was determined by performing tensile tests. The results of the tensile tests allowed us to identify the bonding interface, after which an auger electron spectroscopy (AES) analysis was performed on the fracture surface using an AES analyzer [46]. This offered a much better resolution than the SEM-

ACCEPTED MANUSCRIPT

EDX method. In this way, the relationship between the adhesion strength and the state of the thin natural-oxide film at the interface was evaluated.

2. Experimental Method

2.1. Cold-spray conditions

Water-atomized pure-copper powder (AtW-350, Fukuda, Japan) was used as the deposition material. As shown in **Fig. 2,** the mean diameter of this powder is 37 µm. The substrate material was an aluminum alloy (A5052), with dimensions of 50 × 50 × 15 mm. The substrate was not subjected to grit blasting before spraying. The powder was sprayed onto the substrate using high-pressure cold-spray equipment (PCS-304, Plasma Giken Co., Japan) using nitrogen gas. The gas was at a temperature of 800°C, and a pressure of 3 MPa. The spray distance was maintained at 20-25 mm during spraying. The spray conditions are listed in **Table 1**. A 15-mm deposition was formed on the aluminum substrate as shown in **Fig. 3**. A cross-section of the deposited deposition and substrate interface is shown in **Fig. 4**. The deposition has a very dense structure. Roughness due to particle collision is formed at the interface. Although the interface is almost perfectly joined, some voids are observed immediately below the attached particles. This gap is thought to be a result of the south-pole problem, and is likely to give rise to weak binding.

2.2. Small tensile adhesion test

To perform an elemental analysis of the bonding interface of the CS copper deposition, it is necessary to separate the deposition from the substrate at the bonding interface. The specimens were machined into the dimensions shown in **Fig. 5**. The copper deposit was positioned at the top of the specimen and the aluminum alloy substrate at the bottom. The bonding interface was thus located in the center part of the specimen. The gauge length was 5.23 mm, and the diameter of the gauge was 1.8 mm. Since the average particle diameter of the powder is about 37 µm, the adhesion strength obtained by the small tensile test exhibits sufficient macroscopic characteristics. In this

ACCEPTED MANUSCRIPT

experiment, the adhesion strength was evaluated under a low strain rate of 0.03 mm/min, giving a strain rate of about 10^{-4} s^{-1}.

2.3. Auger electron spectroscopy (AES) analysis

Auger electron spectroscopy (AES) involves accelerated electrons being irradiated onto the specimen such that auger electrons with an intrinsic element energy are released from the surface layer, which is about 0.4–5 nm thick in 50–2500 eV. Auger electrons are detected on the surface of the specimen, which provides information on the type and amount of the element to be analyzed. An AES analysis of a microscopic region of several tens of nm, an analysis of the element in-plane distribution, and the depth direction distribution can be performed. It is possible to analyze the composition of the specimen surface, the component surface of the micro precipitate, and the vicinity of the interface of the sample having a segregated element and film at the interface. As such, this is an effective means of elemental analysis. In the widely used SEM-EDX method, the analysis of the thin oxide film covering the surface is difficult, because it has a low resolution in the depth direction. However, this can be done when using AES. A scanning AES analyzer (SAM 680, ULVAC-PHI, Japan), shown in **Fig. 6,** was used. In this AES system, a uniaxial tensile testing system is connected to an AES analyzer. They are connected in a vacuum, and the tensile-test specimen is transferred to the analysis chamber by the transfer rod. Therefore, it is possible to conduct a material strength test on the tensile tester and observe and elementally analyze the obtained fracture surface without ever exposing it to an oxidizing atmosphere. In the present study, it proved possible to evaluate the extremely thin oxide film remaining at the interface between the substrate and the deposited deposition. Regarding the fracture surface after the tensile test, observation of the surface shape by SEM imaging, and surface element mapping analysis were carried out using the AES apparatus.

ACCEPTED MANUSCRIPT

3. Results and Discussion

3.1. Adhesion strength of cold-sprayed deposition

The small tensile tests were conducted on the CS copper deposit and aluminum substrate interface specimens using the AES analyzer in a vacuum. These all specimens broke with a brittle fracture at the adhesion interface of copper deposit and aluminum substrate. The adhesion strength was calculated from the maximum value of the obtained fracture load, divided by the cross-sectional area of the gauge. The calculated results are listed in **Table 2**. The adhesion strength of the interface was found to be approximately 93 MPa, with very little variation in the strength, which is in good agreement with the results of previous research [44].

3.2. SEM observation of fracture interface

The results of SEM observations of the fracture surface of aluminum substrate side are shown in **Fig. 7**. The fracture surface consisted of a large number of small craters and overall presented a remarkably rough surface. These craters are not due to the characteristics of the metallic materials such as the dimpling caused by the size of the particles or the brittle fracture behavior. Rather, these are impact marks formed by the numerous impacts that occur during spraying. A higher-magnification SEM observation shows that the sizes and shapes of the craters varied considerably.

The copper powder was prepared by a water-atomizing method, giving it irregular shapes and a large particle size distribution. Moreover, since multiple particles are simultaneously ejected from the nozzle, the particles interfere with each other and exhibit a complicated impact behavior.

Furthermore, we focused on one crater of the aluminum substrate side and examined the fracture mode in detail as shown in **Fig.8**. **Fig. 8a** shows the SEM observation results for a crater formed by the collision of a single particle. In the center of the crater, a relatively smooth region can be observed. In contrast, dimples caused by ductile fracture can be confirmed around the outer circumference. These observations confirmed the differences in the adhesion state, even though they addressed only the surface produced by a single particle. We designated the smooth center part

ACCEPTED MANUSCRIPT

"A" and the outer circumference with the dimples "B." The results of observing zone A are shown in **Fig. 8b**, while those for zone B are shown in **Fig. 8c**.

The dimples, which are caused by ductile fracture, cannot be observed in zone A. The evidence of breakage at the time of the tensile test could not be confirmed. Therefore, in the central region of the crater, that is, in the south pole part, almost no chemical bond was formed even if the particles came into contact with the substrate. Alternatively, after rebounding, a part was separated from the substrate to form a void. This is thus a weakly bonded region that does not contribute significantly to the adhesion strength of the overall deposition.

In contrast, based on the results of the observation shown in **Fig. 8b** (zone B), it is possible to divide zone B into two sub-zones according to the bonding state. In the first, a dimple structure peculiar to the ductile fracture surface was observed (B-1). The AES spectrum analysis, described below, of this B-1 dimple structure, revealed that aluminum was the dominant material. Since the dimple structure was also observed at the same position on the deposition side, we can conclude that the Al substrate underwent ductile fracture in this region during the tensile test. This means that the bonding strength of the B-1 zone is greater than the fracture strength of the substrate (A 5052: tensile strength of 175 to 215 MPa). Then, the second region is characterized by small particles remaining on the fracture surface of the substrate (B-2). The particles, which elemental analysis revealed to be copper, remained to the substrate after fracturing in the tensile test. In that region, the substrate oxide film is cracked, and the underlying aluminum is exposed. This result indicates that, in zone B-2, a fresh surface is exposed by the destruction and removal of the oxide film, such that a large bonding strength is achieved between the particles and the substrate so that, even after rupture, particles remain adhered to the substrate. In order to cause fracture failure in the copper deposit and to leave copper fragments on the substrate side, the interfacial strength must be higher than the strength of the copper and the strength of the copper must be lower than the strength of aluminum. This type of fracture was observed only the outer edges of craters. Besides, the thickness of the remaining copper is very thin, and the thickness is close to the fine grain region of the deposited

ACCEPTED MANUSCRIPT

particle. At this location, the angle of the joining surface close to the maximum principal stress direction. Furthermore, it is weak against shear stress due to the refinement of the grain. In some parts of the crater edge where these conditions are met, the fracture occurred in the copper deposit. Therefore, in either B zone, the deposited deposition bonds strongly to the substrate. The reason why only the outer edges of the craters attained a high level of strength will be discussed in the next section, which addresses our evaluation of the remaining oxide film.

3.3. AES evaluation of oxide remaining on deposition interface

An AES mapping analysis was carried out to determine element distribution at the substrate and deposition interface. The analysis was performed for copper, aluminum, and oxygen. The adhesion of the particles at the substrate and deposition interface and the state of the remaining oxide were evaluated. We analyzed not only the substrate but also the deposit at the fracture surface. The AES observation/analysis position can be confirmed by the coordinate information of the electric specimen stage of the AES system, and its coordinates can be represented by angular coordinates distance d from the center of the specimen and angle θ. Therefore, the observation position on the substrate side can be expressed as $d = d_{analysis}$, and $\theta = \theta_{analysis}$. In order to find a place corresponding to the substrate side observation region, we observed the entire circumference of the $d = d_{analysis}$ of the deposit side specimen. From this all circumference observation result, we could find the place that is corresponding by the shape. Detailed analysis and observation were carried out in these places.

The results are shown in **Fig. 9**. In this figure, the mapping result for the substrate is shown on the left-hand side and that for the deposit on the right-hand side. These clearly correspond to each other, with there being a mirror-image relationship.

The crater centers (Zone A) on the substrate exhibit a relatively high oxygen level and large amounts of oxide can be observed. In contrast, the amount of oxygen is observed to be low at the crater outer edges (Zone B) on the substrate, while the copper and aluminum levels are high. This

ACCEPTED MANUSCRIPT

result points to the following phenomenon. Since the oxide film is not destroyed, the particles and base material do not form a chemical bond at the center of the crater. At the outer edges, however, a large shear plastic deformation occurs. Since these damages the oxide film sufficiently, the metal of the particle and substrate bond to each other satisfactorily. These results clearly indicate that the natural oxide film is destroyed by the plastic deformation, and direct contact between the newly generated surfaces are the main factors affecting cold-sprayed deposition.

Even previous research efforts have reported that the degree of plastic deformation is small at the points at which collision occurs, but large enough at the edges to form a material jet [13, 21, 23, 32]. That is, in those regions where the plastic deformation is small, such as at the points at which a collision occurs, the oxide film remains as is and the bonding strength is weak. On the other hand, in those regions where a large plastic deformation occurs, such as where the edge of a particle reaches the substrate, the oxide film is removed to enable the formation of a strong bond, which supports the findings of the present study [34,35].

3.4. Features of well-bonded region

The results of an AES analysis of the substrate and the deposit revealed that the bonding state at the interface between the substrate and cold-spray deposition is not uniform, with there being no bonding in those areas where oxide remains. Since there is a correlation between the remaining amount of oxide and the bonding strength, determining the state of the remaining oxide is important to enabling an understanding of the overall bonding state. In the actual cold-spray process, since the particle size exhibits a distribution and given that the gas flow is non-uniform, the size of the particles, the collision direction, and the collision speed all have a varied distribution. Therefore, the plastic deformation of the particles and the remaining oxide film also vary. In this section, we describe our examination of whether the oxides exhibit a distribution across the entire interface, using SEM observations and AES element mapping.

ACCEPTED MANUSCRIPT

Fig. 10 shows SEM images and AES elemental mapping results for copper, aluminum, and oxygen. The results shown in **Fig. 10** were obtained from the craters on both the substrate and deposit sides. Both evaluation areas correspond to each other, and are mirror-image symmetrical. This figure again shows that the remaining oxide film state is not uniform. Due to the difference in the impact behaviors of the particles, the state of plastic deformation during deposition also differs.

Focusing on the state of the oxide, the state of the oxide remaining on each crater could be divided into three types, as shown in **Fig. 11.**

In region (i), since a large amount of oxide remains in the center of the crater, it can be deduced that there is not much plastic deformation at the point of collision, whereas there are large amounts of plastic deformation around the outer edges of the crater. This corresponds to the ideal deposition behavior where a CS particle perpendicularly impacts a flat substrate. The bonding strength is not actually attained at the point of collision because no newly generated surface is exposed.

In contrast, in region (ii), craters with almost no remaining oxide were found. In this region, since the oxide was essentially entirely removed, allowing the copper to fully bond to the substrate, the resulting bonding strength is expected to better. This adhesion behavior is thought to be due to the overall removal and breaking of the oxide by following two reasons. First, the copper particles used in the present study were irregularly shaped, being prepared by water atomization. There was also a region in which the stress concentrates at the center of the point of collision. Seconds. Multiple collisions of particles may have formed irregularly shaped craters. A remaining oxide film, which could not be removed by the single impact, was entirely removed by the assistance of multiple collisions.

Moreover, craters that were entirely covered in oxide were also identified, as shown in (iii). Because this was often found in the case of the smaller-diameter craters, we can assume that the kinetic energy at the instant of impact was not high enough to remove the oxide film from the substrate. There were some craters that did not exhibit the south-pole problem, as typified by (ii).

ACCEPTED MANUSCRIPT

There is a correlation between the removal amount of the oxide film and the impact velocity of the particles, which dominates the critical velocity of adhesion. Also, in the actual cold spray process, there are variations in the particle velocities, and these variations determine the difference in the state of adhesion of region (i), (ii) and (iii). In the case of the region (i), the single particle impact velocity exceeds the critical deposit condition sufficiently. On the other hand, the region (ii) and (iii) do not exceed the critical condition with a single particle collision. However, in the region (ii), the oxide film is entirely removed by multiple collisions, and make a satisfactory bond.

From these, we can assume that the south-pole problem can be mitigated by controlling the particle collision conditions and oxide film removal by the assistance of multiple collisions, and the other methods such as laser pretreatment.

3.5. Area ratio of well-bonded zone from which oxide is eliminated

The luminance value of the AES mapping analysis represents the intensity of the detected signal. In the mapping results, those areas with a greater amount of a given element have a higher luminance value, and thus appear brighter. To determine that proportion of the area which is bonded, binarization processing is performed to divide the luminance value histogram for oxygen into regions in which the oxide remains and others from which it has been removed. MATLAB R2017a (The MathWorks, Inc., USA) was used for this analysis. **Fig. 12** shows the oxygen mapping results for the substrate of the CS substrate and deposit fracture surface. A histogram of the luminance values obtained for this area is shown in **Fig. 13**. The horizontal axis represents the luminance, and the vertical axis represents the count. The brighter areas have higher luminance count numbers. In this histogram, there are two peaks corresponding to the high-brightness area (oxide-covered region) and low-brightness area (no-oxide region). Since the maximum luminance value was 233, binary processing was performed by adopting, as the threshold value (Th_L) a value of 117 (decimal part rounded up) which is half the maximum value. **Fig. 14** shows a binary image of the AES mapping result for oxygen. The white regions indicate those areas where the oxygen level is low,

ACCEPTED MANUSCRIPT

that is, those regions from which the oxide was removed allowing a strong bond to form. The size of the area from which the oxide had been removed, relative to the overall observation area, was measured by counting the number of pixels in the white part and dividing that by the number of pixels in the entire analysis area. The value obtained for the white area ratio was only 36%, that is, the area in which good bonding was attained was smaller than the oxide-covered area. For this reason, the overall adhesion strength of the deposit is 90 MPa, even though some parts of the region exhibit a bonding strength exceeding the mechanical strength of the substrate. As mentioned above, if we can control the impact conditions, the south-pole problem would be mitigated, thus increasing the size of the area with good bonding and thus improving the adhesion strength.

The above clearly illustrates that the amount of remaining oxide film is a very important factor affecting the adhesion strength of a CS deposition. In the future, we hope to quantitatively understand how the presence or absence of the oxide film affects the CS adhesion strength, by evaluating the local degree of difference in the strength of these weakly bonded well-bonded regions through ultra-small strength evaluation tests [47].

4. Conclusion

The interfacial adhesion strength of a cold-sprayed copper deposition on an aluminum substrate was measured by performing tensile tests. These tests exposed the bonding interface, produced by the adhesion tests, with the results being superior to those of elemental analysis.

Elemental analyses were performed on the fracture surfaces using an AES analyzer, which offers a much better resolution than the SEM-EDX method, and the relationship between the state of the thin natural oxide film at the interface and the adhesion strength was evaluated.

To understand the relationship between the adhesion strength and the oxide film remaining on the surface of the aluminum substrate onto which the copper deposition is cold sprayed, tensile interfacial adhesion strength measurements, AES elemental mapping, and SEM evaluations were carried out. The findings obtained are summarized below:

ACCEPTED MANUSCRIPT

The overall adhesion strength between the CS copper deposit and the aluminum substrate was approximately 93 MPa. Craters of various sizes and shapes are formed at the bonding interface, and the bonding state varies greatly depending on the location. However, within a single crater, the center acts as the south pole and is covered by a native oxide film, hence is not bonded. In contrast, an oxide-free metallic area is found at the edge of each crater, allowing a strong bond to form. Moreover, this region has a strong adhesion strength that exceeds that of the copper deposit. Comparing the sizes of these regions, we found that those where the oxide film had been removed, enabling the formation of a strong bond, were relatively small. Therefore, the overall adhesion strength is smaller than the local strength of the well-bonded region. Given these facts, we can say that the remaining oxide film is one of the key factors affecting the CS deposition mechanism. Also, with some craters, there was no south-pole problem due to the collision history during the cold-spray deposition process. When parameters such as the particle shape and size can be optimized, and the collision state can be controlled and oxide film removal by the assistance of multiple collisions, and the other methods such as laser pretreatment, it is possible to overcome the south-pole problem. Our goal is to overcome the south-pole problem and thus obtain a deposit with a better adhesion strength. Moreover, in the future, we hope to quantitatively understand the effect of the presence or absence of remaining oxide film on the CS adhesion strength.

Acknowledgement

This work was supported by JSPS KAKENHI Grant Number 15H05501.

References

[1] A.P. Alkhimov, V.F. Kosarev, A.N. Papyrin, A method of “cold” gas-dynamic deposition, Phys.-Dokl. 35 (1990) 1047–1049.

[2] A.P. Alkhimov, V.F. Kosarev, A.N. Papyrin, Gas-dynamic spraying. An experimental study of the spraying process, J. Appl. Mech. Tech. Phys. 39 (1998) 318–323. doi:10.1007/BF02468100.

[3] A. Papyrin, COLD SPRAY TECHNOLOGY, Ad. Mater. Processes. 159 (2001) p49–51.

[4] A. Moridi, S.M. Hassani-Gangaraj, M. Guagliano, M. Dao, Cold spray coating: review of material systems and future perspectives, Surf. Eng. 30 (2014) 369–395. doi:10.1179/1743294414Y.0000000270.

ACCEPTED MANUSCRIPT

[5] R.N. Raoelison, C. Verdy, H. Liao, Cold gas dynamic spray additive manufacturing today: Deposit possibilities, technological solutions and viable applications, Mater. Des. 133 (2017) 266–287. doi:10.1016/j.matdes.2017.07.067.

[6] T. Stoltenhoff, H. Kreye, H.J. Richter, An Analysis of the Cold Spray Process and Its Coatings, J. Therm. Spray Technol. 11 (2002) 542–550. doi:10.1361/105996302770348682.

[7] H. Assadi, F. Gärtner, T. Stoltenhoff, H. Kreye, Bonding mechanism in cold gas spraying, Acta Mater. 51 (2003) 4379–4394. doi:10.1016/S1359-6454(03)00274-X.

[8] M. Grujicic, J.R. Saylor, D.E. Beasley, W.S. DeRosset, D. Helfritch, Computational analysis of the interfacial bonding between feed-powder particles and the substrate in the cold-gas dynamic-spray process, Appl. Surf. Sci. 219 (2003) 211–227. doi:10.1016/S0169-4332(03)00643-3.

[9] M. Grujicic, C.L. Zhao, W.S. DeRosset, D. Helfritch, Adiabatic shear instability based mechanism for particles/substrate bonding in the cold-gas dynamic-spray process, Mater. Des. 25 (2004) 681–688. doi:10.1016/j.matdes.2004.03.008.

[10] M. Grujicic, C.L. Zhao, C. Tong, W.S. DeRosset, D. Helfritch, Analysis of the impact velocity of powder particles in the cold-gas dynamic-spray process, Mater. Sci. Eng., A 368 (2004) 222–230. doi:10.1016/j.msea.2003.10.312.

[11] T. Han, Z. Zhao, B.A. Gillispie, J.R. Smith, Effects of Spray Conditions on Coating Formation by the Kinetic Spray Process, J. Therm. Spray Technol. 14 (2005) 373–383. doi:10.1361/105996305X59369.

[12] C.J. Li, W.Y. Li, Y.Y. Wang, G.J. Yang, H. Fukanuma, A theoretical model for prediction of deposition efficiency in cold spraying, Thin Solid Films. 489 (2005) 79–85. doi:10.1016/j.tsf.2005.05.002.

[13] S.V. Klinkov, V.F. Kosarev, M. Rein, Cold spray deposition: Significance of particle impact phenomena, Aerosp. Sci. Technol. 9 (2005) 582–591. doi:10.1016/j.ast.2005.03.005.

[14] J. Wu, H. Fang, S. Yoon, H. Kim, C. Lee, The rebound phenomenon in kinetic spraying deposition, Scr. Mater. 54 (2006) 665–669. doi:10.1016/j.scriptamat.2005.10.028.

[15] T. Novoselova, P. Fox, R. Morgan, WO'Neill, Experimental study of titanium/aluminium deposits produced by cold gas dynamic spray, Surf. Coat. Technol. (2006).

[16] E. Calla, D.G. McCartney, P.H. Shipway, Effect of Deposition Conditions on the Properties and Annealing Behavior of Cold-Sprayed Copper, J. Therm. Spray Technol. 15 (2006) 255–262. doi:10.1361/105996306X108192.

[17] W.Y. Li, H. Liao, C.J. Li, G. Li, C. Coddet, X. Wang, On high velocity impact of micro-sized metallic particles in cold spraying, Appl. Surf. Sci. 253 (2006) 2852–2862.

[18] T. Schmidt, F. Gärtner, H. Assadi, H. Kreye, Development of a generalized parameter window for cold spray deposition, Acta Mater. 54 (2006) 729–742. doi:10.1016/j.actamat.2005.10.005.

[19] G. Bae, Y. Xiong, S. Kumar, K. Kang, C. Lee, General aspects of interface bonding in kinetic sprayed coatings, Acta Mater. 56 (2008) 4858–4868. doi:10.1016/j.actamat.2008.06.003.

[20] G. Bae, S. Kumar, S. Yoon, K. Kang, H. Na, H.J. Kim, et al., Bonding features and associated mechanisms in kinetic sprayed titanium coatings, Acta Mater. 57 (2009) 5654–5666. doi:10.1016/j.actamat.2009.07.061.

[21] S. Guetta, M.H. Berger, F. Borit, V. Guipont, M. Jeandin, M. Boustie, et al., Influence of Particle Velocity on Adhesion of Cold-Sprayed Splats, J. Therm. Spray Technol. 18 (2009) 331–342. doi:10.1007/s11666-009-9327-0.

[22] T. Hussain, D.G. McCartney, P.H. Shipway, D. Zhang, Bonding Mechanisms in Cold Spraying: The Contributions of Metallurgical and Mechanical Components, J. Therm. Spray Technol. 18 (2009) 364–379. doi:10.1007/s11666-009-9298-1.

ACCEPTED MANUSCRIPT

[23] P.C. King, G. Bae, S.H. Zahiri, M. Jahedi, C. Lee, An Experimental and Finite Element Study of Cold Spray Copper Impact onto Two Aluminum Substrates, J. Therm. Spray Technol. 19 (2009) 620–634. doi:10.1007/s11666-009-9454-7.

[24] T. Schmidt, F. Gärtner, H. Assadi, H. Kreye, Development of a generalized parameter window for cold spray deposition, Acta Mater. (2006).

[25] K. Ogawa, K. Ito, K. Ichimura, Y. Ichikawa, Y. Ichikawa, S. Ohno, N. Onda, Characterization of Low-Pressure Cold-Sprayed Aluminum Coatings, J. Therm. Spray Technol. 17 (2008) 728–735. doi:10.1007/s11666-008-9254-5.

[26] T. Schmidt, H. Assadi, F. Gärtner, H. Richter, T. Stoltenhoff, H. Kreye, T. Klassen, From Particle Acceleration to Impact and Bonding in Cold Spraying, J. Therm. Spray Technol. 18 (2009) 794–808. doi:10.1007/s11666-009-9357-7.

[27] M. Fukumoto, M. Mashiko, M. Yamada, E. Yamaguchi, Deposition Behavior of Copper Fine Particles onto Flat Substrate Surface in Cold Spraying, J. Therm. Spray Technol. 19 (2009) 89–94. doi:10.1007/s11666-009-9426-y.

[28] W.Y. Li, C. Zhang, C.J. Li, H. Liao, Modeling Aspects of High Velocity Impact of Particles in Cold Spraying by Explicit Finite Element Analysis, J. Therm. Spray Technol. 18 (2009) 921–933. doi:10.1007/s11666-009-9325-2.

[29] P.C. King, M. Jahedi, Relationship between particle size and deformation in the cold spray process, Appl. Surf. Sci. 256 (2010) 1735–1738. doi:10.1016/j.apsusc.2009.09.104.

[30] P.C. King, C. Busch, T. Kittel-Sherri, M. Jahedi, S. Gulizia, Interface melding in cold spray titanium particle impact, Surf. Coat. Technol. 239 (2014) 191–199. doi:10.1016/j.surfcoat.2013.11.039.

[31] J. Xie, D. Nélias, H. Walter-Le Berre, K. Ogawa, Y. Ichikawa, Simulation of the Cold Spray Particle Deposition Process, J. Tribol. 137 (2015) 041101–041101. doi:10.1115/1.4030257.

[32] H. Assadi, H. Kreye, F. Gartner, T. Klassen, Cold spraying – A materials perspective, Acta Mater. (2016). doi:10.1016/j.actamat.2016.06.034.

[33] C. Chen, Y. Xie, R. Huang, S. Deng, Z. Ren, H. Liao, On the role of oxide film's cleaning effect into the metallurgical bonding during cold spray, Mater. Lett. 210 (2018) 199–202. doi:10.1016/j.matlet.2017.09.024.

[34] W.Y. Li, W. Gao, Some aspects on 3D numerical modeling of high velocity impact of particles in cold spraying by explicit finite element analysis, Appl. Surf. Sci. 255 (2009) 7878–7892. doi:10.1016/j.apsusc.2009.04.135.

[35] Y. Ichikawa, K. Ogawa, Effect of Substrate Surface Oxide Film Thickness on Deposition Behavior and Deposition Efficiency in the Cold Spray ProcessYuji Ichikawa & Kazuhiro Ogawa, J. Therm. Spray Technol. (2015) 1–10. doi:10.1007/s11666-015-0299-y.

[36] D. Zhang, P.H. Shipway, D.G. McCartney, Cold Gas Dynamic Spraying of Aluminum: The Role of Substrate Characteristics in Deposit Formation, J. Therm. Spray Technol. 14 (2005) 109–116. doi:10.1361/10599630522666.

[37] C.J. Li, H.T. Wang, Q. Zhang, G.J. Yang, W.Y. Li, H.L. Liao, Influence of Spray Materials and Their Surface Oxidation on the Critical Velocity in Cold Spraying, J. Therm. Spray Technol. 19 (2009) 95–101. doi:10.1007/s11666-009-9427-x.

[38] K. Kim, W. Li, X. Guo, Detection of oxygen at the interface and its effect on strain, stress, and temperature at the interface between cold sprayed aluminum and steel substrate, Appl. Surf. Sci. 357 (2015) 1720–1726. doi:10.1016/j.apsusc.2015.10.022.

[39] Y. Ichikawa, K. Ogawa, Critical Deposition Condition of CoNiCrAlY Cold Spray Based on Particle Deformation Behavior, J. Therm. Spray Technol. 26 (2016) 340–349. doi:10.1007/s11666-016-0477-6.

[40] P.C. King, S.H. Zahiri, M. Jahedi, Microstructural Refinement within a Cold-Sprayed Copper Particle, Metall. Mater. Trans. A. 40 (2009) 2115–2123. doi:10.1007/s11661-009-9882-5.

ACCEPTED MANUSCRIPT

[41] J. Villafuerte, Modern Cold Spray, Springer International Publishing, Cham, 2015. doi:10.1007/978-3-319-16772-5.

[42] J.I. Goldstein, D.E. Newbury, P. Echlin, D.C. Joy, C.E. Lyman, E. Lifshin, et al., Scanning Electron Microscopy and X-ray Microanalysis, Springer US, Boston, 2003. doi:10.1007/978-1-4615-0215-9.

[43] T. Hussain, D.G. McCartney, P.H. Shipway, Impact phenomena in cold-spraying of titanium onto various ferrous alloys, Surf. Coat. Technol. 205 (2011) 5021–5027. doi:10.1016/j.surfcoat.2011.05.003.

[44] R. Huang, H. Fukanuma, Study of the Influence of Particle Velocity on Adhesive Strength of Cold Spray Deposits, J. Therm. Spray Technol. 21 (2011) 541–549. doi:10.1007/s11666-011-9707-0.

[45] A.M. Birt, V.K. Champagne Jr, R.D. Sisson Jr, D. Apelian, Microstructural Analysis of Cold-Sprayed Ti-6Al-4V at the Micro- and Nano-Scale, J. Therm. Spray Technol. (2015) 1–12. doi:10.1007/s11666-015-0288-1.

[46] S. Hofmann, Auger- and X-Ray Photoelectron Spectroscopy in Materials Science, Springer-Verlag Berlin Heidelberg, Heidelberg, 2013. doi:10.1007/978-3-642-27381-0.

[47] Y. Ichikawa, R. Tokoro, K. Ogawa, Micro-Scale Strength Evaluation for Bonding Interface of Cold Sprayed Coatings, Mater. Sci. Forum. 879 (2016) 795–800. doi:10.4028/www.scientific.net/MSF.879.795.

ACCEPTED MANUSCRIPT

ACCEPTED MANUSCRIPT

ACCEPTED MANUSCRIPT

ACCEPTED MANUSCRIPT

Table 1 Cold-spray conditions.

Equipment	PCS-304 (Plasma Giken Co., Japan)
Gas	
Type	Nitrogen
Pressure	3 MPa
Temperature	800 °C
Spray Distance	20–25 mm
Traverse speed	20 mm/s
Powder	
Material	Pure Copper (AtW-350, Fukuda, Japan)
Mean diameter	37 µm
Process	Water atomized
Substrate	
Material	Aluminum A5052

ACCEPTED MANUSCRIPT

ACCEPTED MANUSCRIPT

Table 2 Results of tensile adhesion tests.

Specimen	**Adhesion strength**
No. 1	85 MPa
No. 2	90 MPa
No. 3	103 MPa
Average	**92.7 MPa**
Standard deviation	**9.29**

ACCEPTED MANUSCRIPT

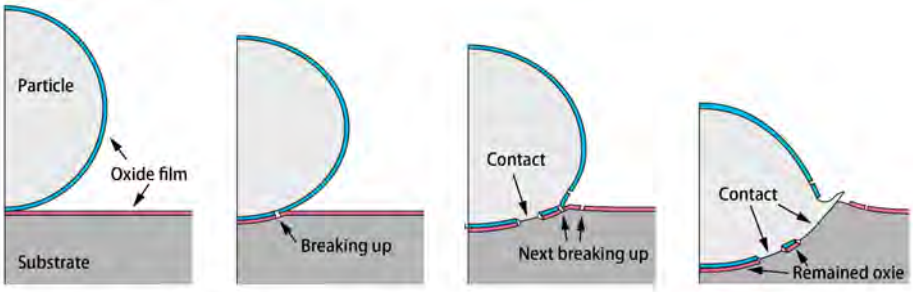

Fig. 1 Deformation of particle upon impact, and break-up of oxide films. [34]

ACCEPTED MANUS

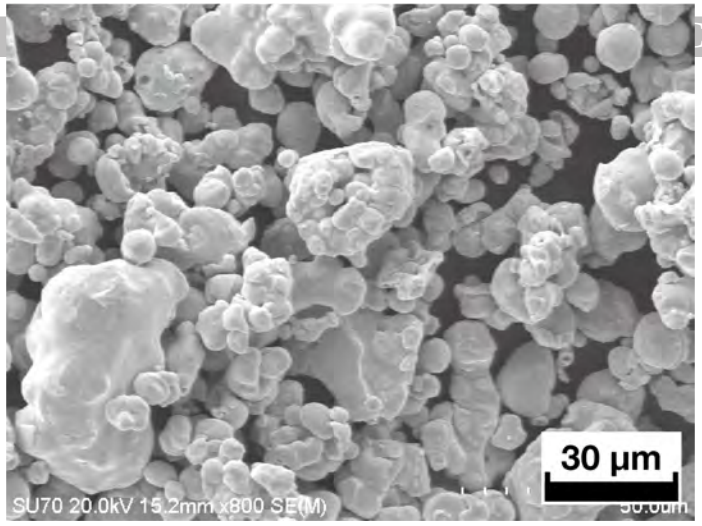

Fig. 2 SEM image of copper powder.

Comment [YI1]: [Response 5]
In order to clear the size of powder, the SEM image is exchanged.

ACCEPTED MANUS

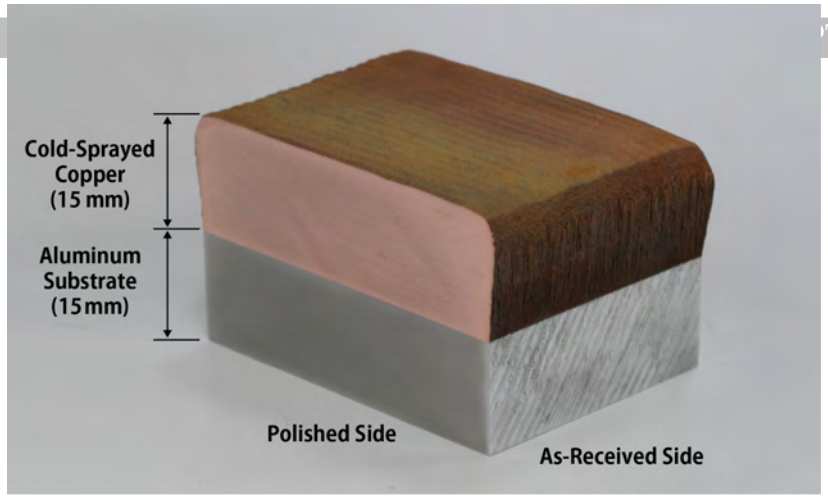

Fig. 3 Cold-sprayed copper deposited on aluminum substrate.

ACCEPTED MANUS

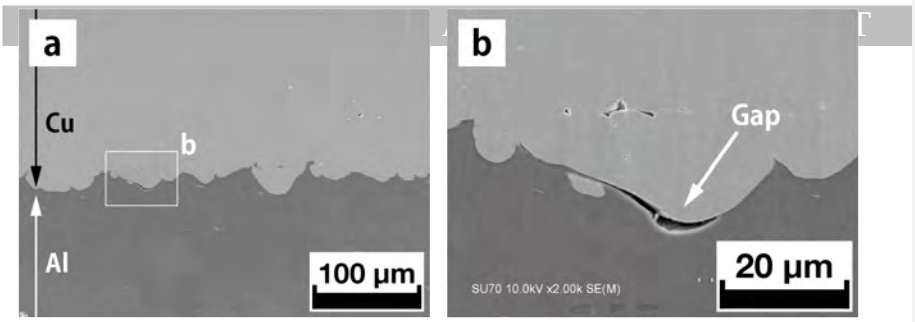

Fig. 4 Typical cross-sectional SEM image of interface between cold-sprayed copper deposit and aluminum substrate, a) lower magnified view, b) higher magnified image of gaped interface between substrate and attached particle.

ACCEPTED MANUS

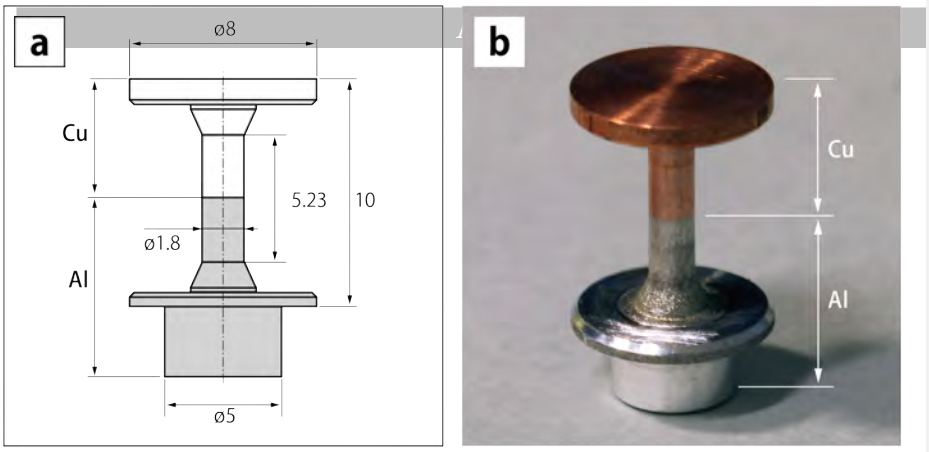

Fig. 5 Detail of small tensile adhesion strength specimen. The adhesion test was performed in a high-vacuum AES chamber connected to the tensile testing system, a) schematic and b) images of the specimen.

ACCEPTED MANUS

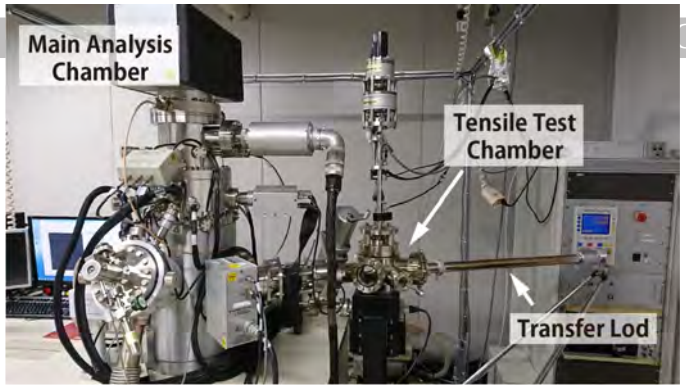

Fig. 6 High-vacuum tensile testing system connected to AES apparatus.

ACCEPTED MANUS

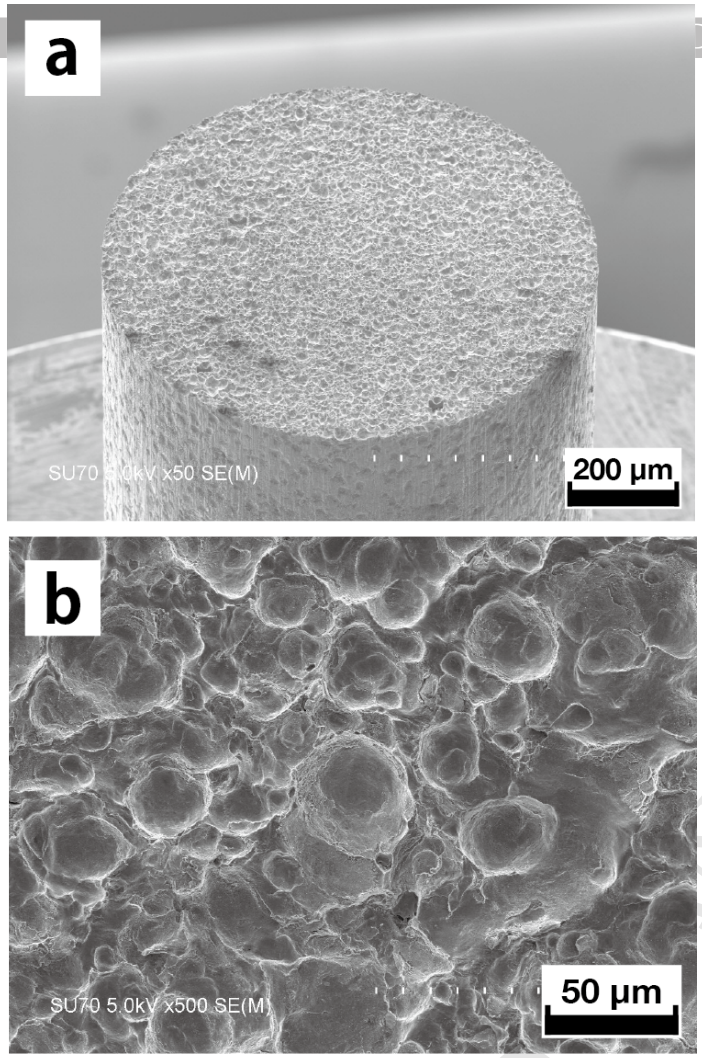

Fig. 7 SEM image of fracture surface of the aluminum substrate side. (a) Low-magnification image of overall fracture interface, (b) magnified collision craters.

Comment [YI2]: [Response 7]
We indicate the image is substrate side.

ACCEPTED MANUS

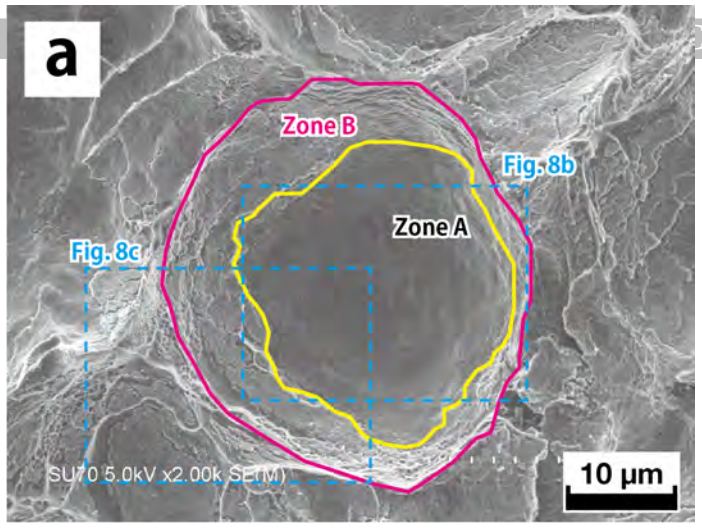

ACCEPTED MANUS

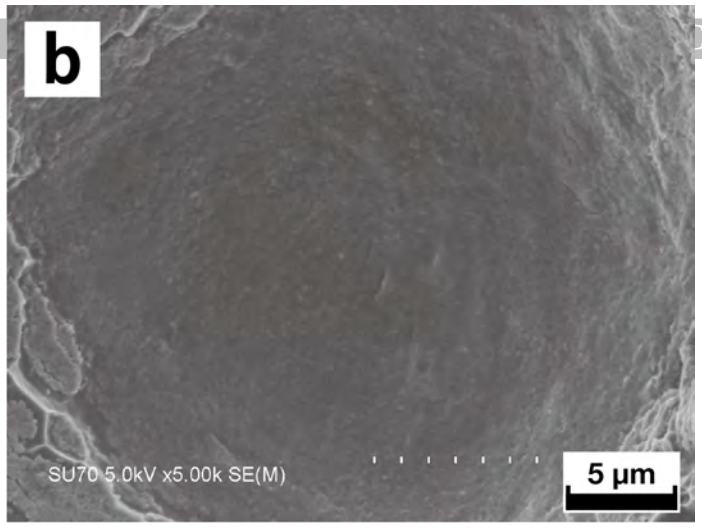

ACCEPTED MANUS

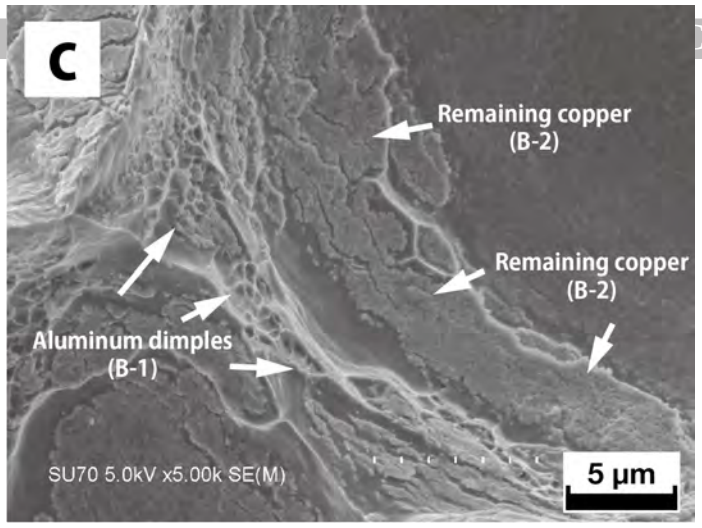

Fig. 8 SEM observation results of collision crater of the aluminum substrate side, that corresponds to following AES evaluation. (a) overall evaluated crater, (b) higher-magnification image of center of impact crater, (c) higher-magnification image of edge of impact crater.

Comment [YI3]: [Response 7]
We indicate the image is substrate side.

ACCEPTED MANUS

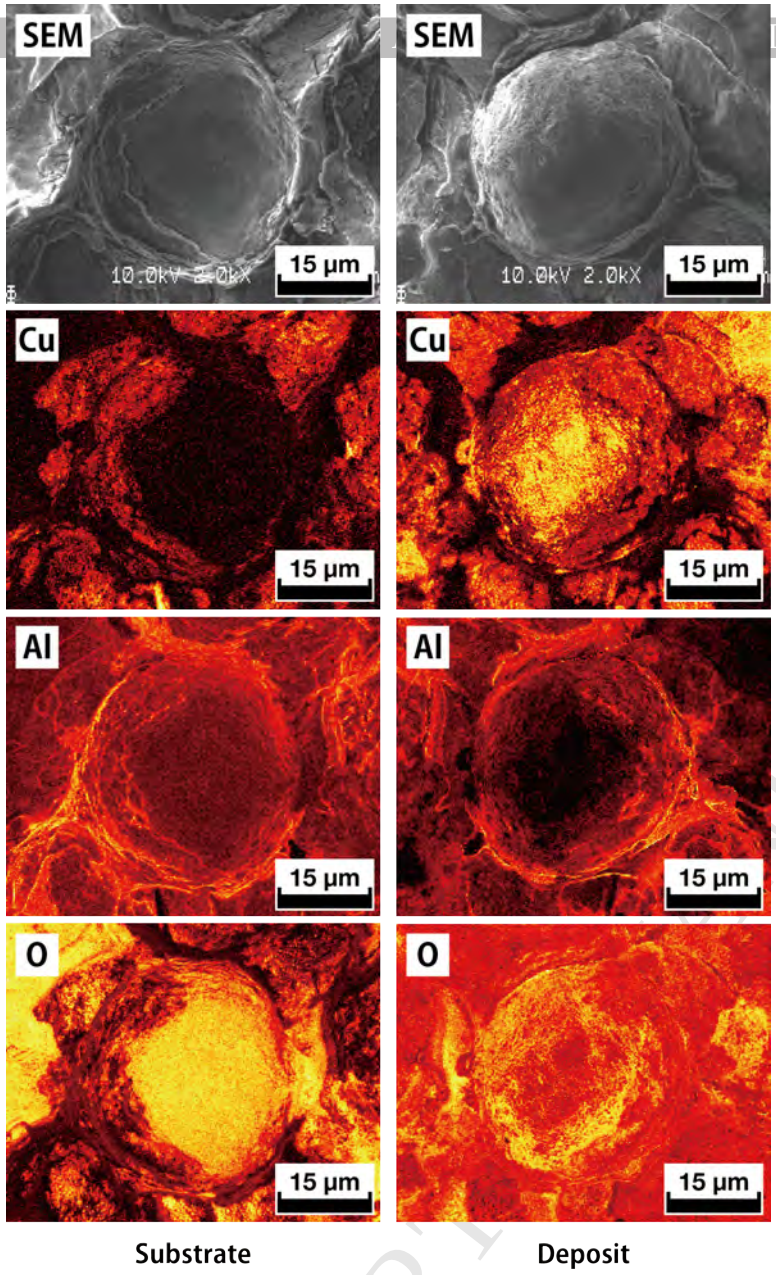

Fig. 9 SEM image and AES mapping results of fracture interface between substrate craters and deposition particles.

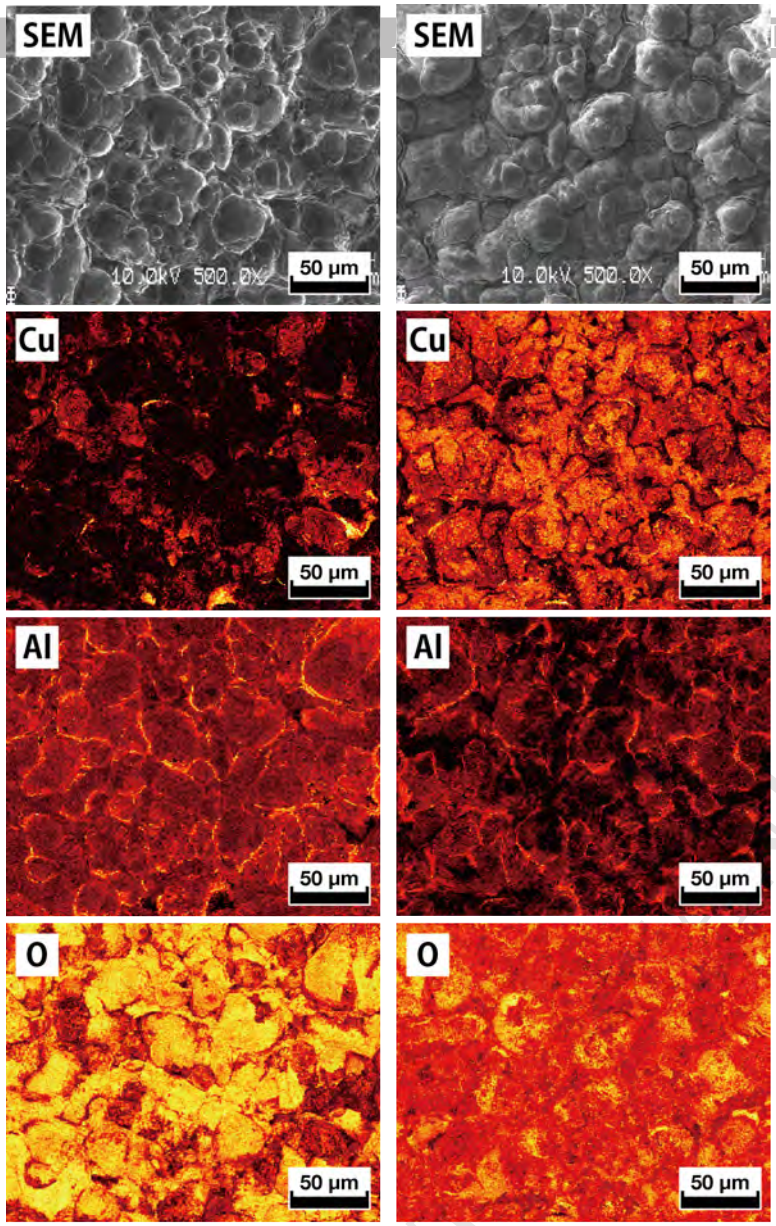

Fig. 10 SEM image and AES mapping results of fracture interface between substrate and deposit.

ACCEPTED MANUSCRIPT

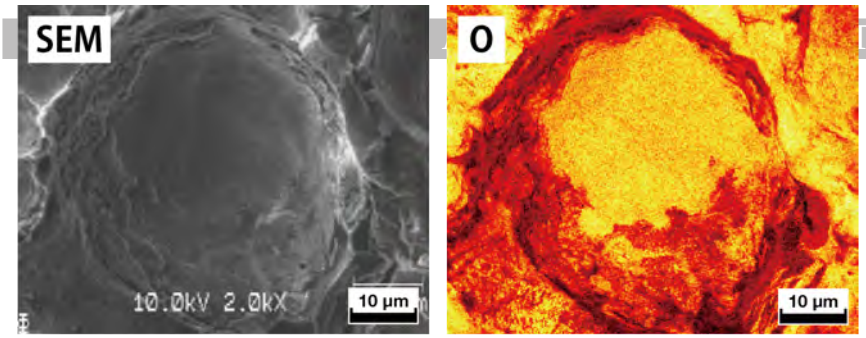

(a) Oxide exists mainly in center of crater

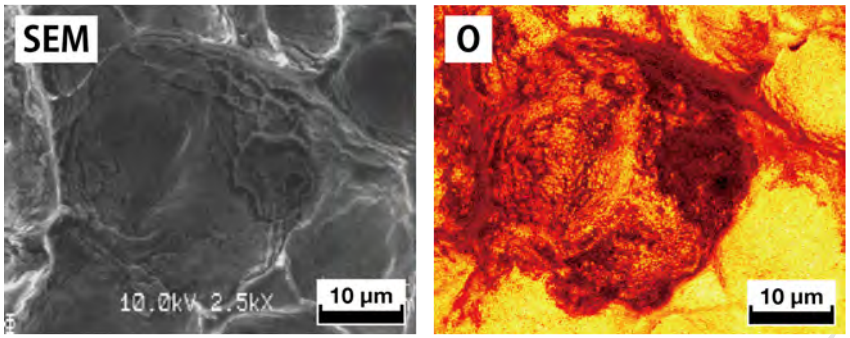

(b) No oxide in crater

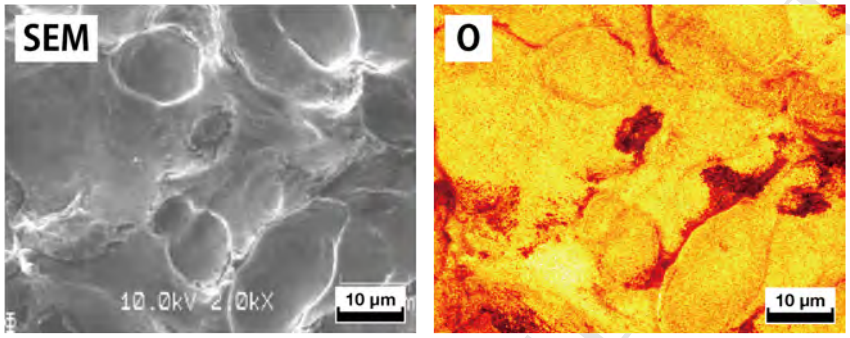

(c) Oxide covers entire crater

Fig. 11 Three different oxide covering patterns for crater.

ACCEPTED MANUSCRIPT

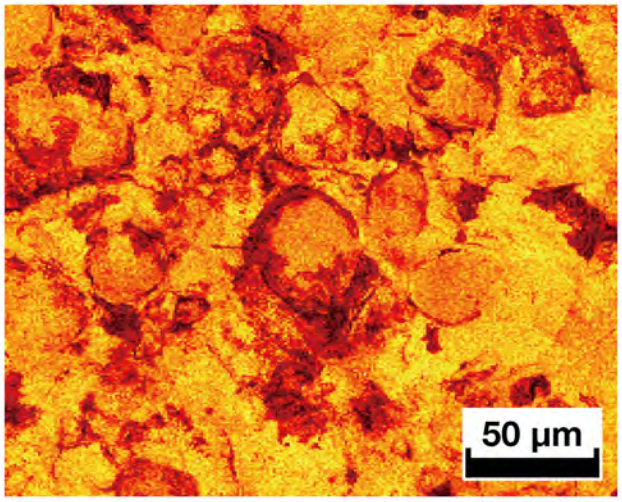

Fig. 12 Oxygen AES mapping result for the fracture surface of substrate.

ACCEPTED MANUS

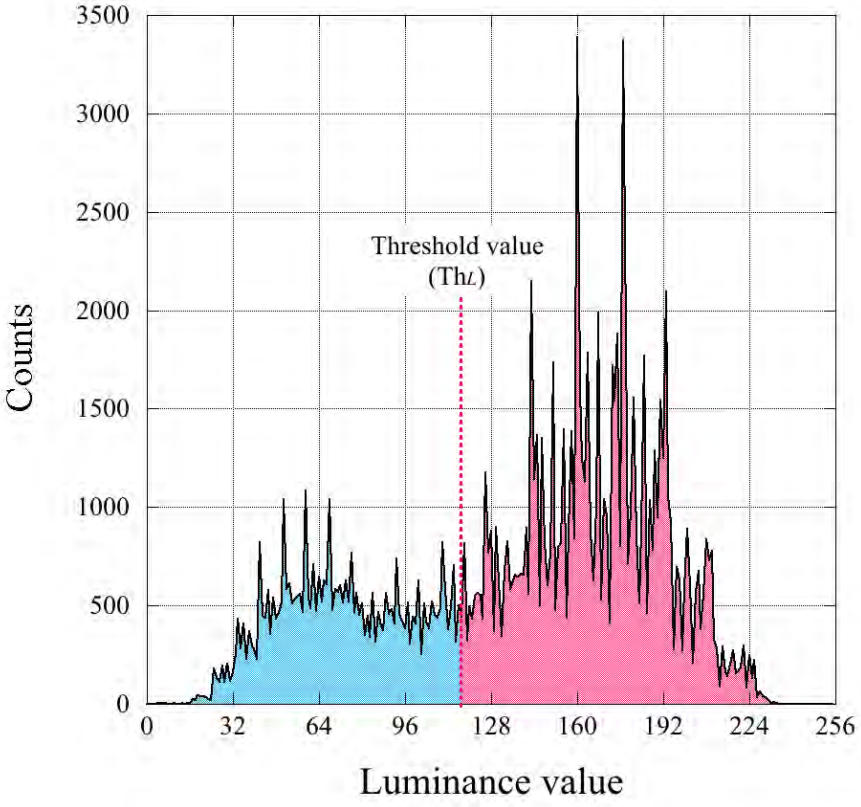

Fig. 13 AES signal intensity luminance histogram and threshold value of binary processing.

ACCEPTED MANUSCRIPT

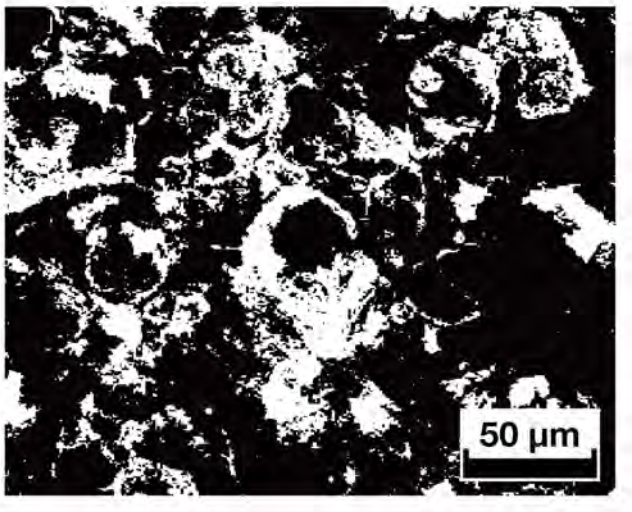

Fig. 14 Binary AES mapping result for oxygen corresponding to Fig. 13. The white parts are those regions from which the oxide has been removed.

ACCEPTED MANUS